Lipid Tubule Self-Assembly: Length Dependence on Cooling Rate Through a First-Order Phase Transition

Britt N. Thomas,* Cyrus R. Safinya, Robert J. Plano, Noel A. Clark

The formation kinetics and self-assembly of multilamellar tubules of the diacetylenic phospholipid 1,2-bis(tricosa-10,12-diynoyl)-*sn*-glycerol-3-phosphocholine formed under controlled cooling rates were studied by x-ray diffraction and optical, atomic force, and scanning electron microscopy. Tubule formation was driven by a reversible first-order phase transition from an intralamellar, chain-melted L_α phase to a chain-frozen $L_{\beta'}$ phase. These observations are the basis of a highly efficient method of tubule production in which tubule lengths can be controlled, between 1 and 100 micrometers, by varying the cooling rate. These tubules can be made in suspensions with 10 percent lipid by mass, far exceeding the lipid solubility limit.

Saturated ethanol-water solutions of the synthetic diacetylenic phospholipid 1,2-bis(tricosa-10,12-diynoyl)-*sn*-glycerol-3-phosphocholine spontaneously self-assemble to produce vesicles with a highly unusual cylindrical structure upon cooling, as reported by Yager and co-workers (*1*, *2*) in 1984. The cylindrical multibilayer vesicles, referred to as "tubules," are typically several tens of micrometers in length, are just under 1 μm in diameter, and have a hollow center (Fig. 1A). Since their discovery, their morphology, size, and hollowness, combined with the ability to control and enhance the mechanical rigidity of the tubule through cross-linking of the molecule's polymerizable diacetylene moieties, have led researchers to suggest numerous technical applications (*3*). These include chemical encapsulation and controlled release, separations, and nano- and microscale electronic and magnetic applications of metallized tubules (*3*–*5*).

We present here the results of a detailed study of the tubule self-assembly process and have developed and used a tubule generation technique such that x-ray diffraction can be used to dynamically probe the kinetics of tubule formation. These x-ray experiments reveal the phase coexistence of lamellar chain-melted L_α and chain-frozen $L_{\beta'}$ phases at the tubule formation temperature. High-resolution, synchrotron-based scattering shows that the lamellar correlations are finite in range but extend over many layers; the correlation distances are on the order of 0.5 μm in the high-temperature (spherical) phase and up to 0.15 μm in the low-temperature (tubule) phase. Interlamellar positional correlations, present in desiccated tubules (*6*), are absent in hydrated tubules, indicating that tubule formation is essentially a first-order intralamellar chain-freezing phase transition, that is, a consequence of passage through the Krafft temperature. Optical microscopy shows the corresponding mesoscopic structural change from fluid-layer spherical multilamellar vesicles (MLVs) in the high-temperature phase to crystalline-layer tubular multilamellar vesicles (tubules) in the low-temperature phase.

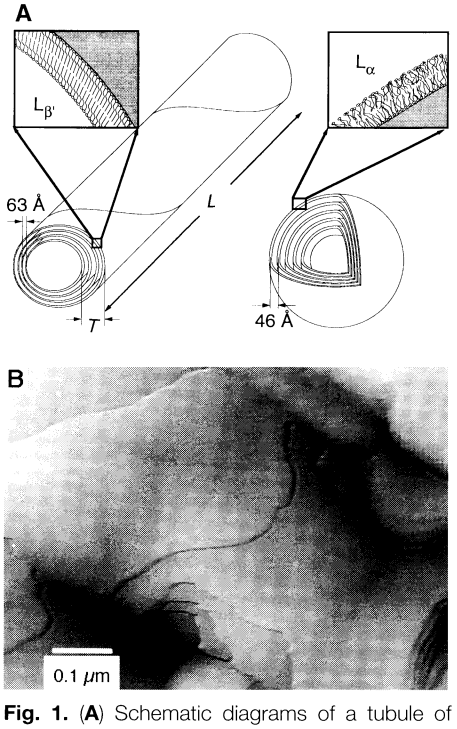

Fig. 1. (**A**) Schematic diagrams of a tubule of length *L*, diameter *D*, and wall thickness *T* (left), and of a fluid-layer spherical MLV (right). (**B**) An atomic force micrograph of a fractured tubule, in which four distinct lamellar layers are revealed.

The first-order nature of this transition suggests that control of the cooling rate determines the tubule morphology, as is commonly found for first-order crystallizations. Indeed, Caffrey *et al.* (*7*) have noticed such a correlation between cooling rate and tubule length. Consequently, by using optical, atomic force, and electron microscopy, we have studied the structure and dimensions of the tubules formed over a wide range of cooling rates, from as slow as 0.08°C per hour to 10^5 °C per hour, the latter attained by liquid N_2 quenching. A technique for controlling tubule dimensions by varying the cooling rate was developed that made it possible to prepare tubules of selectable mean length *L* at lipid concentrations up to 20 times that previously possible. Interestingly, the tubule diameter was only a weak function of cooling rate or tubule length. These observations permit us to speculate on the various theories of tubule formation, which we discuss below. Earlier studies (*3*, *8*) concerning the manipulation of the external dimensions of tubules have relied on varying the solvent composition in which the tubules are formed; substitution of methanol or propanol for ethanol shifts the narrow distribution of tubule lengths from an average of ~40 ± 10 μm in a 1-propanol–water solvent to ~65 ± 10 μm for a methanol-water solvent. Furthermore, tubules generated in methanolic solvent systems tend to be monolamellar, whereas tubules formed in other alcohol solvent systems under otherwise identical conditions tend to be multilamellar.

Our method for the initial preparation of tubules is as follows: A solution of lipid concentration c = 1 mg/ml was prepared in ethanol:water [75:25 (v:v)], was heated with vigorous stirring to 55°C to dissolve the lipid, and then was allowed to cool to room temperature; this yielded a flocculent precipitate of tubules (typically with $L \approx 20$ μm and diameter $D \approx 1$ μm). This precipitate was centrifuged at 10,000*g* at 5°C for 30 min; optical microscopy of the resulting pellet revealed no discernible change in tubule morphology induced by centrifugation. This concentrated paste, typically with c = 100 mg of lipid per milliliter, was then heated to 38.5°C, whereupon it entered the MLV phase. It was then cooled to 36.0°C at a constant rate R to regenerate tubules.

If the temperature of the MLV suspension exceeded 50°C, the opaque off-white paste abruptly became transparent, indicating MLV disruption. So long as the MLV integrity was maintained, one could revers-

B. N. Thomas, Condensed Matter Laboratory, Department of Physics, University of Colorado, Boulder, CO 80309, and Exxon Research and Engineering Company, Annandale, NJ 08801, USA.
C. R. Safinya, Materials and Physics Departments and the Interdepartmental Program on Biochemistry and Molecular Biology, University of California, Santa Barbara, CA 93106, USA.
R. J. Plano, Exxon Research and Engineering Company, Annandale, NJ 08801, USA.
N A. Clark, Condensed Matter Laboratory, Department of Physics, University of Colorado, Boulder, CO 80309, USA.
*To whom correspondence should be addressed.

ibly cycle through the MLV-to-tubule transition by heating and cooling with a concentration of 100 mg of lipid per milliliter. For samples driven above 50°C, the products formed upon cooling depended on the lipid concentration: As expected, dilute samples ($c < 5$ mg/ml) yielded a preponderance of tubules, but when $c \approx 5$ mg/ml, a mixture of tubules and irregular lipid plaquettes was obtained, and when $c \gg 5$ mg/ml, only plaquettes were produced.

The multilamellar character of tubules generated in ethanolic solutions is demonstrated in the atomic force micrograph of a fractured tubule (Fig. 1B). Three distinct lamellar steps of approximately 65 Å can be seen in the direction normal to the tubule axis. The multilamellar character of the tubule can also be clearly seen in the coaxial cylindrical lamellae at the tubule end. Lower magnification electron microscopy reveals that the lamellae are helically wound to form the cylinders (*3*).

Stringent control of R through the MLV-to-tubule phase transition determines the final external tubule dimensions. Remarkably, we obtained tubules throughout the range 0.0825°C/hour $< R <$ 10^5 °C/hour. However, their lengths varied widely, as can be seen in optical microscopy images of fully hydrated tubules subjected to the MLV-to-tubule phase transition with R = 0.08°C/hour (Fig. 2A), R = 10°C/hour (Fig. 2B), and those subjected to a liquid N_2 quench (Fig. 2C).

The large disparity between L and D required that we use optical and scanning electron microscopy, respectively, to determine these values (9). For each determination of L or D, a minimum of 350 measurements were made; for all rates R, the L distributions resembled Boltzmann distributions, but the D distributions were very narrow and essentially symmetric about the mean value. We found that, between the extremes of the liquid N_2 quench and controlled cooling at R = 0.0825°C/hour, D varied from 0.70 μm (σ_D = 0.15 μm) to 1.08 μm (σ_D = 0.3 μm). A far more dramatic increase was found in the mean tubule length L for these two preparations: L = 3.86 μm (σ_L = 2.27 μm) for the liquid N_2–quenched preparation whereas L = 50.6 μm (σ_L = 23.9 μm) was found for R = 0.0825°C/hour. The relation between L and R is shown in Fig. 3A. For $c \approx 1$ mg/ml and $R \approx$ 0.1°C/hour, mean lengths >150 μm could be attained.

Our discovery that the MLV-to-tubule phase transition occurs at $c \approx 100$ mg of lipid per milliliter made possible kinetic examination of the phase transition by x-ray diffraction. Small-angle, high-resolution x-ray scattering from the vesicles yielded not only the interlamellar repeat distances for the tubule and MLV phases, but also the relative concentrations of the different phases and the smectic layering and correlation lengths (that is, the spatial extent over which the interlamellar spacing remained in registry). High-angle x-ray scattering revealed the nature of the ordering of the molecular arrangement within the bilayer membranes.

Tubule samples of $c \approx 100$ mg of lipid per milliliter were placed in standard 1.5-mm quartz diffraction capillaries, yielding unoriented powder samples. Several low-resolution x-ray diffraction scans from a single concentrated tubule preparation, driven between 34° and 37°C, are shown in Fig. 4. Two phases appear to coexist through the phase transition, and the reversibility of the phase transition is immediately apparent. Also discernible from this sequence of low-resolution diffraction scans is a pronounced temperature hysteresis of the cycle; whereas the low-q [$q = 4\pi/\lambda \sin(2\theta/2)$, where λ is the x-ray wavelength and 2θ is the scattering angle], low-temperature phase has essentially disappeared at 36.25°C, in the cooling portion of the cycle it does not emerge until about 35.25°C. The first and last scans in Fig. 4 were taken 14 hours apart. The coexistence of two phases and the hysteresis further indicate that the tubule-to-MLV phase transition is first-order. As the length of the lipid chain is ≈28 Å, the surprisingly small interlayer spacing d = 47.6 Å ($d = 2\pi/q_{MLV}$; q_{MLV} = 0.132 Å) in the chain-melted MLV phase is indicative of bilayer interdigitation. The interdigitation disappears in the crystalline tubule phase where the tubule peak at 0.095 $Å^{-1}$, corresponding to an interlayer spacing of 66.105 Å, is consistent with bilayers consisting of tilted chain-frozen lipids, as we discuss below. Such interdigitation has been observed in liposomes composed of pure DPPC, DSPC, and DMPC in ethanolic solutions (*10*).

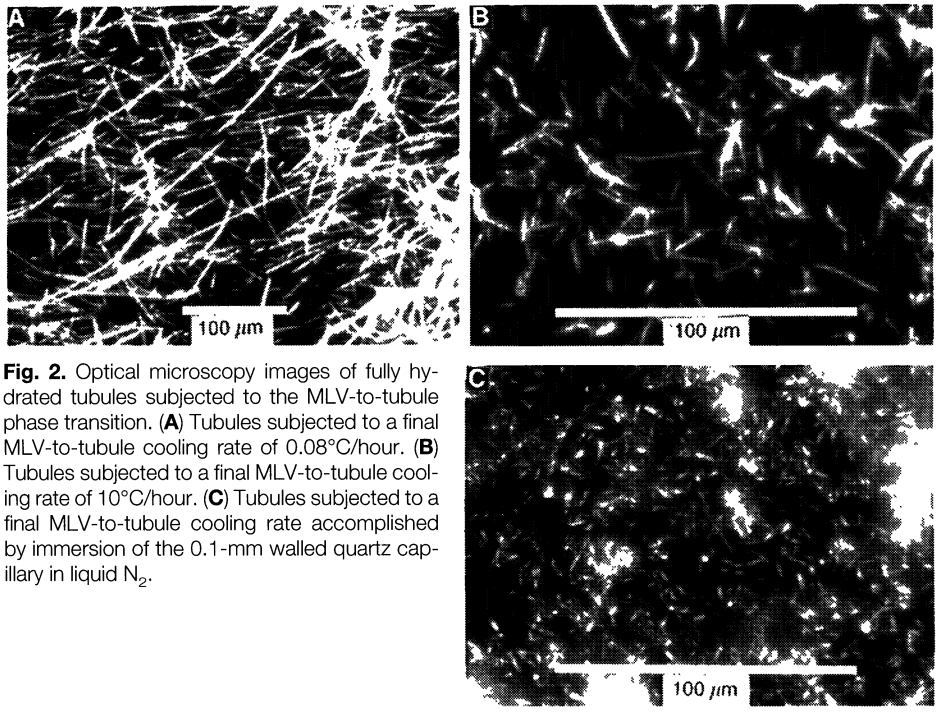

Fig. 2. Optical microscopy images of fully hydrated tubules subjected to the MLV-to-tubule phase transition. (**A**) Tubules subjected to a final MLV-to-tubule cooling rate of 0.08°C/hour. (**B**) Tubules subjected to a final MLV-to-tubule cooling rate of 10°C/hour. (**C**) Tubules subjected to a final MLV-to-tubule cooling rate accomplished by immersion of the 0.1-mm walled quartz capillary in liquid N_2.

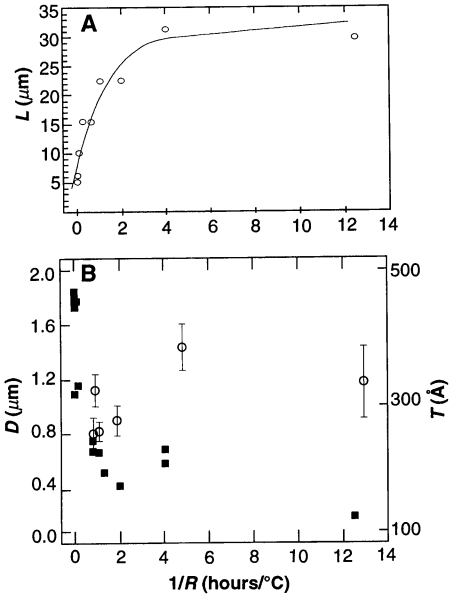

Fig. 3. (**A**) Relation between mean tubule length L and the inverse of the cooling rate, $1/R$, through the transition from spherical vesicle to tubule phase. All points on this plot arise from the same lipid concentration, ~100 mg of lipid per milliliter of solvent. The line is merely a guide to the eye. (**B**) Plot of $1/R$ versus tubule mean diameter D (open circles) (left scale) and versus tubule wall thickness T (filled squares) (right scale).

The nature of the in-plane hydrocarbon chain ordering was explored by x-ray scans in the high–wave-vector range plotted in Fig. 5. The MLV phase is characterized by a broad liquid structure factor peaked at $q = 1.5$ Å^{-1}, indicating that the hydrocarbon chains are in an L_α-like fluid phase. Upon cooling to the tubule phase, the onset of a sharp peak ($q = 1.37$ Å^{-1}) on the lower side of this broad peak of the liquid structure factor indicates the commonly observed lipid bilayer $L_{\beta'}$ structure factor in which the ordered tilted chains pack in a distorted hexagonal lattice (*11–15*). Three distinct $L_{\beta'}$ phases are known to exist (*11–13*): The $L_{\beta I}$, $L_{\beta F}$, and $L_{\beta L}$ designations specify whether the tilt of the hydrocarbon chain is toward the nearest neighboring chain, the next-nearest neighbor, or at an angle between these two, respectively. The differences between x-ray data for the three $L_{\beta'}$ phases are unambiguous only in oriented lamellar samples (*13–15*); the powder nature of our samples thereby prevents us from distinguishing among these.

High-resolution synchrotron x-ray diffraction scans taken at low angles enabled us to determine the extent of layering correlation from the width of the (00ℓ) layer stacking Bragg peaks. In the tubule phase, the correlation length is governed by the thickness T of the tubule wall. The inset to Fig. 4 shows two typical high-resolution scans through the (00ℓ) stacking peaks emanating from a single preparation in the tubule (at 36.0°C) and the MLV (at 36.9°C) phases. The (00ℓ) peak is clearly much narrower in the spherical MLV phase than in the tubule phase. Fitting the data to a model appropriate for stacked, rigid multimembrane lyotropic systems (*16*) yielded correlation lengths on the order of 0.5 μm; a model consisting of discrete concentric spherical shells yielded a length of 0.56 μm. We observed a slight dependence of these values on the tubule-to-MLV melting rate, with lower rates yielding slightly larger MLVs.

The tubule phase (00ℓ) peak was fitted to the powder average of the scattering from infinite length multilayer tubule structures having outer diameter D, wall thickness T, and layer spacing d. The nested layers were assumed to be perfect cylinders corresponding to membranes with no bending fluctuations, that is, rigid membranes (*17*). From the model and the measured half-width at half-maximum, we obtained a thickness T that we take to be the mean tubule thickness, a reasonable assumption because D is rather narrowly distributed for a given value of R. We found that the increases in T from 0.068 to 0.135 μm between the liquid N_2 quench and our slowest cooled sample lags significantly behind the corresponding increase in D from 0.70 to 1.08 μm. That is, the inner tubule diameter ($D - 2T$) increases and the tubule becomes more hollow as L increases (Fig. 3B).

These data indicate that the process of formation of multilamellar tubules is driven by a first-order freezing transition involving in-plane two-dimensional (2D) ordering. Phase contrast microscopy indicates that the basic tubule structure is established during this 2D freezing process, the ordered state growing as narrow bilayer ribbons, which spontaneously curl because of the system chirality. The ribbons are therefore kinetically determined structures, growth forms that can be expected to depend on the cooling rate, system composition, impurity content, and degree of supersaturation or undercooling, in ways similar to those found for the growth of 3D crystals. We have not attempted any theoretical analyses of these freezing kinetics; however, it is possible that the ribbon shape may be related to conditions of equilibrium.

Existing theories (*18–21*) have described the equilibrium structure of monolamellar vesicles. We are concerned here with the formation kinetics of more structurally complex multilamellar vesicles. Cognizant of these discrepancies, we note that early theoretical treatments of tubules predicted a dependence $D \propto L^{1/2}$ or $D \propto L^{1/3}$, whereas more recent theories (*19–21*) that couple molecular tilt and molecular chirality yield either no dependence of D on L or a very weak logarithmic increase of D with L. Our observations of the tubule mean length and mean diameter show almost no dependence of D on L and are most consistent with the Helfrich-Prost (*20*) and Selinger-Schnur (*22*) treatments.

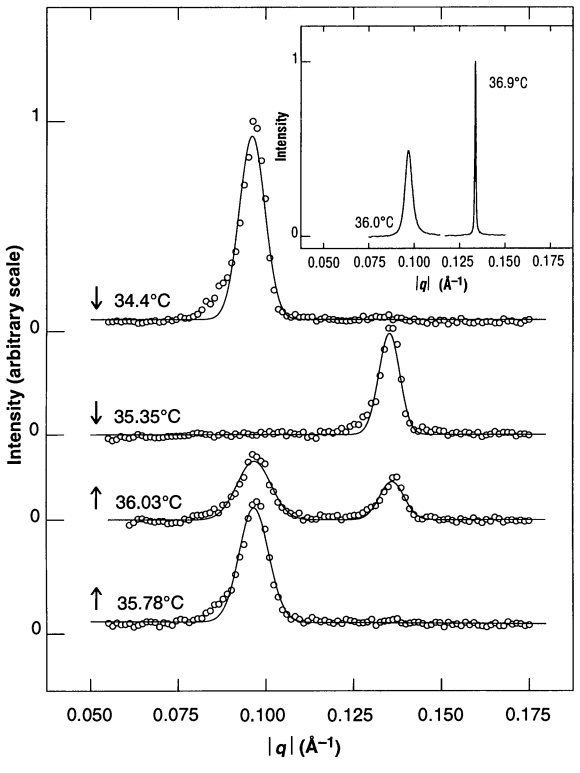

Fig. 4. A sequence of low-resolution (focusing graphite monochromator) x-ray diffraction scans emanating from a single concentrated (100 mg of lipid per milliliter of solvent) tubule sample as it is cycled from the tubule to the MLV and back to the tubule phase. The scan sequence goes from bottom to top; the scans are drawn to the same scale but are offset vertically for clarity. Upward and downward arrows preceding the temperature annotation indicate whether the scan was acquired while heating (tubule-to-MLV transition) or cooling (the MLV-to-tubule transition), respectively. (**Inset**) The corresponding high-resolution sychrotron diffraction results, drawn to a different scale.

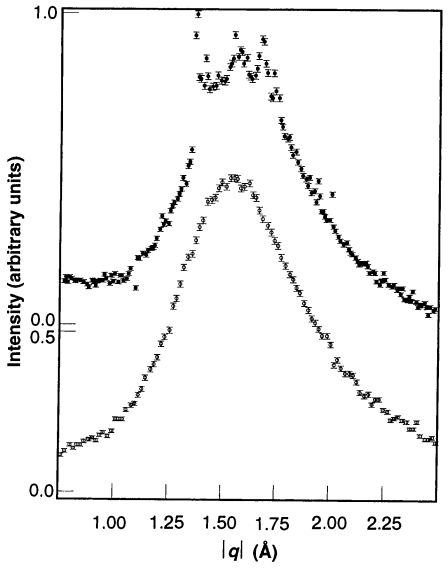

Fig. 5. X-ray data in the large-wave-vector range in the high-temperature MLV (lower curve, white circles) and low-temperature tubule phase (upper curve, black circles). The two curves are drawn to slightly different vertical scales and are vertically offset for clarity. The onset of the sharp peak on the low-angle side of the broad peak indicates the onset of bilayer lipid chain ordering as discussed in the text.

REFERENCES AND NOTES

1. P. Yager and P. Schoen, *Mol. Cryst. Liq. Cryst.* **106**, 371 (1984).
2. _____, C. Davies, R. Price, A. Singh, *Biophys. J.* **48**, 899 (1985).
3. For a recent review, see J. M. Schnur, *Science* **262**, 1669 (1993).
4. D. D. Archibald and S. Mann, *Nature* **364**, 430 (1993).
5. R. Dagani, *Chem. Eng. News* **71**, 19 (9 August 1993).
6. B. N. Thomas *et al.*, *Mater. Res. Soc. Symp. Proc.* **248**, 83 (1992).
7. M. Caffrey, J. Hogan, A. S. Rudolph, *Biochemistry* **30**, 2134 (1991).
8. B. Ratna *et al.*, *Chem. Phys. Lipids* **63**, 47 (1992).
9. The in vacuo conditions required for electron microscopy may exaggerate the measured tubule diameter as a result of flattening upon interlamellar solvent evaporation. The upper limit of distortion for a completely collapsed, infinitely elastic monolamellar tubule is the factor of $(\pi D)/2$, where D is the hydrated tubule diameter.
10. See, for example, S. Nir, J. Bentz, J. Wilschut, N. Duzgunes, *Prog. Surf. Sci.* **13**, 1 (1983). DPPC, DSPC, and DMPC are dipalmitoylphosphatidylcholine, distearoylphosphatidycholine, and dimyristoylphosphatidylcholine, respectively.
11. V. Luzzati, *Biol. Membr.* **1**, 71 (1968).
12. A. Tardieu *et al.*, *J. Mol. Biol.* **75**, 711 (1973).
13. M. J. Janiak, D. M. Smalley, G. G. Shipley, *J. Biol. Chem.* **254**, 6068 (1979).
14. G. S. Smith, E. B. Sirota, C. R. Safinya, N. A. Clark, *Phys. Rev. Lett.* **60**, 813 (1988).
15. E. B. Sirota *et al.*, *Science* **242**, 1406 (1988).
16. G. S. Smith, E. B. Sirota, C. R. Safinya, R. J. Plano, N. A. Clark, *J. Chem. Phys.* **92**, 4519 (1990).
17. C. R. Safinya *et al.*, *Phys. Rev. Lett.* **57**, 2718 (1986); D. Roux and C. R. Safinya, *J. Phys. (Paris)* **49**, 307 (1988).
18. P. G. De Gennes, *C. R. Acad. Sci.* **304**, 259 (1987).
19. T. C. Lubensky and J. Prost, *J. Phys. II (Paris)* **2**, 371 (1992).
20. W. Helfrich and J. Prost, *Phys. Rev. A* **38**, 3065, (1988).
21. Z.-C. Ou-Yang and L.-X. Liu, *Phys. Rev. Lett.* **65**, 1679 (1990); *Phys. Rev. A* **43**, 6826 (1991).
22. J. V. Selinger and J. M. Schnur, *Phys. Rev. Lett.* **71**, 4091 (1993).

23. We gratefully acknowledge useful conversations with R. Shashidar, B. Ratna, E. B. Sirota, and P. Pincus. We thank R. Shashidar for providing the phospholipid. Portions of this work were executed at beamlines X10A and X10B of the National Synchrotron Light Source at Brookhaven National Laboratory, administered by the Department of Energy. B.N.T. and N.A.C. were supported in part by National Science Foundation (NSF) grant DMR 92-23729 to N.A.C. C.R.S. was supported in part by NSF grants DMR-92-21742 and DMR-93-01199 and the Petroleum Research Fund (grant 27837-AC7). B.N.T. thanks the Exxon Research and Engineering Company for their generous extension of office space, x-ray facilities, microscopy, and computing equipment.

12 October 1994; accepted 19 January 1995

Crystal Structure and Function of the Isoniazid Target of *Mycobacterium tuberculosis*

Andréa Dessen,* Annaïk Quémard,* John S. Blanchard,† William R. Jacobs Jr., James C. Sacchettini†

Resistance to isoniazid in *Mycobacterium tuberculosis* can be mediated by substitution of alanine for serine 94 in the InhA protein, the drug's primary target. InhA was shown to catalyze the β-nicotinamide adenine dinucleotide (NADH)–specific reduction of 2-*trans*-enoyl–acyl carrier protein, an essential step in fatty acid elongation. Kinetic analyses suggested that isoniazid resistance is due to a decreased affinity of the mutant protein for NADH. The three-dimensional structures of wild-type and mutant InhA, refined to 2.2 and 2.7 angstroms, respectively, revealed that drug resistance is directly related to a perturbation in the hydrogen-bonding network that stabilizes NADH binding.

Isoniazid has been a first-line chemotherapeutic in the treatment of tuberculosis since 1952 (*1*) but is ineffective against newly emergent strains of *Mycobacterium tuberculosis* that have shown themselves to be drug-resistant. Such strains cause mortality in 70 to 90% of AIDS-stricken patients who develop tuberculosis (*2*). Isoniazid is believed to kill mycobacteria by inhibiting the biosynthesis of mycolic acids—long-chain α-branched β-hydroxy fatty acids that are critical components of the mycobacterial cell wall (*3*). In 25 to 50% of isoniazid-resistant strains, drug resistance is associated with a loss of catalase and peroxidase activities, both of which are encoded by the *katG* gene (*4*, *5*). These activities are thought to participate in the drug sensitivity mechanism by converting isoniazid in vivo into its biologically active form, which then acts on its intracellular target (*6*).

Genetic studies have identified the protein product of the *inhA* gene as the primary target for the action of isoniazid and ethionamide, a closely related chemical analog. Notably, 20 to 25% of isoniazid-resistant clinical isolates display mutations in the *inhA* locus, and substitutions within the *inhA* open reading frame have been shown to express the $Ser^{94} \rightarrow Ala^{94}$ (S94A) and $Ile^{16} \rightarrow Thr^{16}$ (I16T) InhA enzymes (*5*, *7*, *8*).

InhA from *M. tuberculosis* displays 32% amino acid identity with enoyl–acyl carrier protein (ACP) reductase of *Brassica napus* and 40% identity with EnvM from *Escherichia coli* (*5*, *7*–*9*). EnvM is the target of a group of antibacterial compounds, the diazaborines (*9*, *10*), and has been shown to catalyze the reduction of crotonoyl-ACP (*11*). A $Gly^{93} \rightarrow Ser^{93}$ mutation in EnvM, which maps four amino acids from Ser^{94} in the corresponding InhA sequence (*7*), leads to a diazaborine-resistant phenotype (*10*). Thus, Gly^{93} (EnvM) and Ser^{94} (InhA) may lie in analogous regions of the proteins, and the drug resistance mechanisms may share some similarities. A mechanism for diazaborine inhibition of EnvM has recently been proposed (*11*). Here we describe biochemical and structural features of InhA that provide insight into the molecular mechanism of isoniazid resistance.

To determine the biochemical properties of InhA, we subcloned the *inhA* gene into a T7-based vector, overexpressed the protein product in *E. coli*, and purified the product by classic protein purification methods done at 4°C. The purity and size of recombinant InhA were determined by liquid chromatography–electrospray mass spectrometry (LC-MS) (*12*). By following the oxidation of NADH by means of a spectrophotometric assay, we showed that InhA catalyzed the reduction of 2-*trans*-octenoyl-ACP, thus identifying the *inhA* gene product as an enoyl-ACP reductase (Table 1). This result is consistent with the suggestion that InhA participates in mycolic acid biosynthesis (*7*). Enoyl-ACP reduction was linearly dependent on the concentration of added InhA. The kinetic values for InhA were similar to steady-state Michaelis constants for NADH and crotonoyl-ACP exhibited by the *B. napus* enoyl-ACP reductase (*13*). Neither isoniazid nor ethionamide bound to InhA, as assessed by titration microcalorimetry (*14*), which suggests that the drugs must be activated before binding.

We also expressed and purified the S94A form of InhA in an identical manner to that used for the wild-type protein. Kinetic evaluation of the S94A InhA-catalyzed reduction of 2-*trans*-octenoyl-ACP by NADH revealed that the values for the K_m and V_{max} of the enoyl substrate did not differ significantly from the wild-type values; however, the Michaelis constant for NADH was five times higher in the S94A mutant (Table 1). This observation suggested that the mechanism of drug resistance may be related to specific interactions between enzyme and cofactor within the NADH binding site.

To explore the structural basis of this difference, we prepared crystals of recombinant wild-type and S94A InhA in the pres-

A. Dessen, J. S. Blanchard, J. C. Sacchettini, Department of Biochemistry, Albert Einstein College of Medicine, 1300 Morris Park Avenue, Bronx, NY 10461, USA. A. Quémard and W. R. Jacobs Jr., Departments of Microbiology and Immunology and Howard Hughes Medical Institute, Albert Einstein College of Medicine, Bronx, NY 10461, USA.

*These authors contributed equally to this work.
†To whom correspondence should be addressed.